JAAS

PAPER

View Article Online
View Journal

Check for updates

Cite this: DOI: 10.1039/d5ja00481k

Quantification of trace iodine using laser-induced breakdown spectroscopy for real-time monitoring of nuclear off-gas streams†

Hunter B. Andrews, *[a] Zechariah B. Kitzhaber, [a] Chase C. Cobble,[b] Joanna McFarlane [b] and Katherine R. Johnson [b]

This study evaluated the potential of laser-induced breakdown spectroscopy (LIBS) for real-time monitoring of trace gas-phase iodine, which is an element of high significance in nuclear applications due to its long radioactive half-life (as iodine-129), volatility, and biological impact. In anticipation of iodine evolving into off-gas systems in molten salt reactor and nuclear fuel recycling applications, this research aimed to assess LIBS performance in flowing argon and helium matrices; optimize measurement parameters using a multichannel spectrometer; and perform calibrations to assess predictive capabilities and limits of detection (LODs). Experimental results successfully measured gas-phase iodine in flowing argon and helium; however, trace iodine was not detected in air. Optimal delay times were determined to be 10 μs for argon and 1 μs for helium, which are consistent with the expected shorter plasma lifetime in helium relative to argon. An emission line survey was provided with the 206.16, 804.37, 902.24, and 905.83 nm peaks, which were identified as the strongest emission peaks. Calibration models were successfully built in both helium and argon, achieving LODs down to 3 ppm in helium and 5 ppm in argon. The iodine emission at 905.83 nm emerged as the most robust for calibration and was subsequently applied to a time series dataset in argon. The predictive trace confirmed the feasibility of employing LIBS for continuous, online quantification of trace iodine in flowing gas systems.

Received 1st December 2025
Accepted 2nd January 2026

DOI: 10.1039/d5ja00481k

rsc.li/jaas

Open Access Article. Published on 13 January 2026. Downloaded on 2/25/2026 11:40:18 AM.
This article is licensed under a Creative Commons Attribution-NonCommercial 3.0 Unported Licence.

Introduction

Advanced nuclear power is rising in interest to meet the growing need for electricity generation. The molten salt reactor (MSR) is one of the advanced reactor designs gaining attention due to its high efficiencies, passive safety features, and ability to remove radioisotopes online. Unlike traditional nuclear reactors with solid fuel, an MSR uses nuclear fuel dissolved into the liquid salt coolant, which circulates through the primary reactor loop. Because the fuel is dissolved, volatile fission products, such as noble gases, tritium, and iodine, are released from the salt into the inert gas headspace.[1] These off-gas streams require various treatment systems to remove hazardous isotopes from the gas phase and prevent release to the environment. Similar systems are needed for nuclear fuel recycling facilities in which volatile fission products will evolve into the gas phase during dissolution or treatment of used fuel.

Radioactive iodine (iodine-129) is of significant interest in off-gas streams due to its high volatility, high biological activity, and long half-life (1.57×10^7 years). The US Environmental Protection Agency regulations for nuclear power operations in Title 40 of the *US Code of Federal Regulations* (CFR), Part 190, necessitate efficient capture of krypton-85 and iodine-129 before releasing gas streams to the environment.[2] This requirement has motivated a depth of research on effective abatement of iodine from gas streams using caustic scrubbing[3] or solid sorbent materials.[4–6] Unfortunately, options are limited for monitoring the iodine concentration in the gas phase of these experiments; for further details the readers are directed to a recent review on iodine analytical techniques from Riley *et al.*[7] These options are limited even further when considering monitoring off-gas streams *in situ* at industrial MSR or reprocessing facilities.

Previous work on real-time monitoring of molten salt off-gas streams has focused on using optical spectroscopy techniques.[8] Several studies from Kireev *et al.* have utilized laser-induced fluorescence to detect ultra-trace concentrations of gas-phase

[a]*Radioisotope Science and Technology Division, Oak Ridge National Laboratory, Oak Ridge, Tennessee, USA. E-mail: andrewshb@ornl.gov*

[b]*Nuclear Energy and Fuel Cycle Division, Oak Ridge National Laboratory, Oak Ridge, Tennessee, USA*

† This manuscript has been authored by UT-Battelle, LLC, under contract DE-AC05-00OR22725 with the US Department of Energy (DOE). The US government retains and the publisher, by accepting the article for publication, acknowledges that the US government retains a nonexclusive, paid-up, irrevocable, worldwide license to publish or reproduce the published form of this manuscript, or allow others to do so, for US government purposes. DOE will provide public access to these results of federally sponsored research in accordance with the DOE Public Access Plan (https://energy.gov/downloads/doe-public-access-plan).

Open Access Article. Published on 13 January 2026. Downloaded on 2/25/2026 11:40:18 AM. This article is licensed under a Creative Commons Attribution-NonCommercial 3.0 Unported Licence.

iodine and to be able to distinguish different isotopologues.[9–11] Laser-induced fluorescence provided high fidelity molecular concentration information, but depending on the analyte may need specific wavelength lasers resulting in a very targeted analytical system. Raman spectroscopy also offers insight into the molecular form of the species in the off-gas stream (*e.g.*, molecular iodine *versus* iodine monochloride) through measuring vibrational bands, which could be beneficial for understanding the chemistry of the off-gas. Felmy *et al.* demonstrated the ability to monitor gas-phase molecular iodine (I_2) using Raman and fluorescence spectroscopies in a static gas cell.[12] In that study, 532 and 671 nm excitation wavelengths were investigated for Raman measurements, along with chemometric modeling. These standard Raman wavelengths also resulted in iodine fluorescence, which when used with chemometric modeling resulted in limits of detection (LODs) down to 6.7×10^{-5} torr. A complementary technique to Raman is laser-induced breakdown spectroscopy (LIBS). LIBS is performed by focusing a pulsed laser into a sample stream to generate a microplasma.[13] The optical emissions of this plasma are then measured to provide an elemental spectrum regardless of molecular form. Thus, tandem Raman/LIBS measurement modalities provide an understanding of molecular speciation or concentrations and total elemental composition.

Although LIBS is typically referenced as being simultaneously sensitive to nearly all elements, its application to halogens is diminished. This lower detection is caused by challenges associated with the excitation of halogen elements related to their ionization energies.[14] Furthermore, the strongest emission peaks for most halogens fall in the deep ultraviolet (UV) wavelengths that are difficult to measure outside of reduced pressures and vacuum.[15,16] To the authors' knowledge, only a few studies on the measurement of gas-phase iodine have been performed. Zhang *et al.* investigated the quantification of iodine using LIBS in a static low-pressure cell (700 Pa) by comparing nanosecond and picosecond lasers and using the deep-UV 183 nm iodine emission.[17] The result was an excellent LOD for trace iodine at 60 ppb in nitrogen bulk gas. A separate study by Zhang *et al.* measured the signatures of volatile iodomethane. Many iodine emissions were detected, including peaks from singly ionized iodine; however, this gas stream was more concentrated in iodine than monitoring conditions would be.[18] Poole and Hawari recently demonstrated the possibility of monitoring various concentrations of iodine in an argon bulk gas.[19] Their work was performed by flushing argon through a Parr reactor containing volatilized iodine and directing the flow through a gas LIBS cell. One approach typically used for measuring halogens using LIBS is the formation of diatomic molecules in the plasma, which then become excited and are more easily detected. Gaft *et al.* successfully demonstrated measuring iodine through the formation of calcium iodide and barium iodide in the plasma plume; however, these were solid samples in which adding calcium is simple, whereas additions to flowing gas systems are complicated and may have downstream consequences associated with the added elements.[20]

Previous work at Oak Ridge National Laboratory established a mobile gas LIBS platform for monitoring various laboratory systems and demonstrated its use for monitoring noble gases and molten salt aerosols, which are expected in an MSR off-gas stream.[21–23] These studies used a compact multichannel spectrometer to assess LODs for a robust and easily deployable system. The present study was performed to (1) investigate the feasibility of trace gas-phase iodine detection using LIBS in flowing air, argon, and He; (2) optimize LIBS settings for trace gas-phase iodine detection using LIBS; and (3) perform quantitative calibrations in various flowing bulk gases to assess LODs for online monitoring applications using the same compact spectrometer. The ability to monitor iodine in tests representative of MSRs or reprocessing systems represents an important step to meet monitoring needs to aid facilities in adhering to 40 CFR Part 190 requirements.

Experimental

LIBS equipment

LIBS measurements were performed using a customized gas LIBS system outfitted onto a mobile platform. A nanosecond pulsed Nd:YAG laser (Nano-200LG, Litron) with a maximum pulse energy of 200 mJ per pulse was operated at 20 Hz. The laser was fired through a beam expansion module and then focused through an angled window into a gas cell. A gas stream was flowed through the gas cell; a nozzle was used to focus the gas precisely to the laser focal point. A larger-diameter tube was used as the gas cell outlet to provide a sudden expansion configuration to maintain gas velocity through the cell. This experimental setup is amenable to online monitoring by continuously flowing sample gases at atmospheric pressure. Plasma emissions were measured using multiple collection optics located in an array around the laser focal lens. Six fiber optics, configured for their respective wavelength ranges, were used to route collected light to a multichannel spectrometer with broad wavelength coverage (six-channel AvaSpec 4096CL, Avantes). A schematic of the LIBS setup is shown in Fig. 1.

Iodine off-gas testing and abatement laboratory

The mobile LIBS system was transported to the Iodine Off-Gas Testing and Abatement Laboratory across the US Department of Energy's Oak Ridge National Laboratory campus for measurements. Gas sample streams containing trace iodine (*e.g.*, <100 ppm) were made using high-purity helium (99.9%, Airgas), high-purity argon (99.9%, Airgas), and compressed air carrier gases. The compressed air was passed through packed bed desiccant columns to remove excess moisture, resulting in an average of 103 ppm H_2O for the duration of the test. The iodine-bearing gases were generated by passing the carrier gas through a temperature-controlled packed bed containing elemental iodine set to 18 °C. All flow rates were controlled using mass flow controllers (SmartTrak, Sierra Instruments). Iodine concentrations in the gas stream were controlled by varying the flow rate through the packed bed and using a diluting gas at the bed outlet. The total flow rate to the LIBS instrument was held constant at nominally 6.3 L min^{-1}. A schematic of the experimental setup is shown in Fig. 1.

Open Access Article. Published on 13 January 2026. Downloaded on 2/25/2026 11:40:18 AM.
This article is licensed under a Creative Commons Attribution-NonCommercial 3.0 Unported Licence.

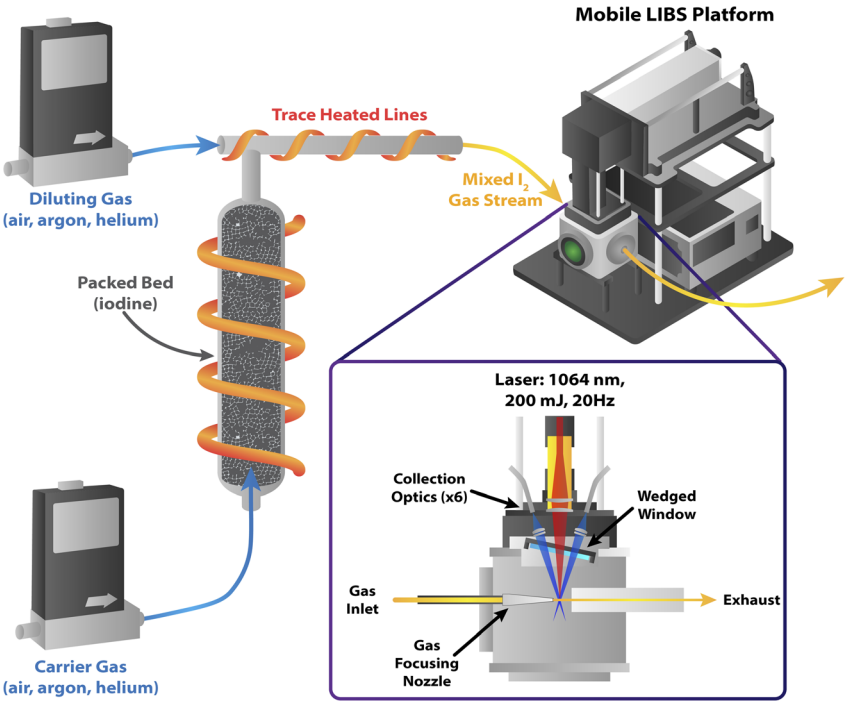

Fig. 1 Diagram of the experimental setup for LIBS measurements of iodine-bearing gases.

Data analysis

Data analysis was performed using Python 3. The optimal LIBS collection settings (*i.e.*, delay time) were determined by maximizing the signal-to-noise ratio (SNR) of the strongest iodine emission peak.[24] The SNR was calculated as

$$\mathrm{SNR} = \frac{\mathrm{signal}}{\mathrm{noise}}, \quad (1)$$

where the signal is the peak area of an emission peak, and the noise is the standard deviation within a nearby spectral window without an emission peak.

LIBS univariate models were constructed by regressing peak areas against concentration. Peak areas were calculated using Simpson integration between two selected wavelength values. Calibration models were evaluated based on their coefficient of regression (R^2) and root mean square error of the calibration (RMSEC). The R^2 represents the variance of the peak intensities that is explained by the concentration variable in the regression model. The RMSEC, which represents the prediction capabilities, is defined as

$$\mathrm{RMSEC} = \sqrt{\frac{\sum (x_i - \hat{x}_i)^2}{n}}, \quad (2)$$

where x_i is the known concentration, $\hat{x}_i$ is the model-predicted concentration, and n is the total number of samples. Because RMSEC metrics are in units of concentration, it is often useful to convert RMSEC values into percent RMSEC (% RMSEC) by normalizing the values to the midpoint concentration used in the calibration. In previous online monitoring studies, model efficacy was ranked using % RMSEC values, classifying them as strong (% RMSEC $\leq$ 5%), satisfactory (5% < % RMSEC $\leq$ 10%), or indicative (10% < % RMSEC $\leq$ 15%).[25]

The LODs and limits of quantification (LOQs) were determined using the 95% prediction intervals of the linear model, as described by Mermet.[26] In the present study, the LOD was determined using the horizontal intersection of the fitted regression line and the upper prediction band value at a concentration of zero. The LOQ was determined similarly but using the horizontal intersection of the upper prediction band value at a concentration of zero and the lower prediction band. The benefit of this approach is that the uncertainty from the entire regression is considered rather than just the sensitivity factor and variance in the blank signal.

Results and discussion

Iodine LIBS spectra in various bulk gases

Electron beam excitation has suggested that the bulk gas can be important to the deep UV spectroscopy of iodine in the many applications where iodine monitoring is of interest.[27] Given the minimal literature on gas-phase iodine detection using LIBS, a survey of emission lines was conducted for iodine in air, helium, and argon. Identified peaks for iodine at trace concentrations are presented in Table 1. The peaks are listed with their relative intensities in each bulk gas, along with their relevant transition properties (A), energy levels (E), and degeneracies (g) as reported in the NIST Atomic Spectra Database.[15,16] The strongest iodine emission peak was identified at 905.83 nm and had no interferences with helium or argon (Fig. 2). Figures highlighting additional identified peaks are provided in the SI. Weaker emission peaks at 804.37, 902.24, 911.89, and

Open Access Article. Published on 13 January 2026. Downloaded on 2/25/2026 11:40:18 AM.
This article is licensed under a Creative Commons Attribution-NonCommercial 3.0 Unported Licence.

Table 1 Identified strongest emission lines for detection of trace-level iodine in argon and helium

Ion	λ (nm)	Relative intensity (Argon)[a]	Relative intensity (Helium)[a]	A (10^8 s^{-1})	E_{low} (eV)	E_{high} (eV)	g_{low}	g_{high}
I	206.16	0.02	0.01	0.13	0.942 649	6.954 610	2	4
I	804.37	0.11	0.11	0.06	6.773 664	8.314 624	6	4
I	902.24	0.05	0.03	0.22	7.550 151	8.923 960	2	4
I	905.83	1.00	1.00	0.32	6.773 664	8.142 020	6	8
I	911.89	—	0.02	0.25	6.954 610	8.314 624	4	4
I	912.80	—	0.02	0.07	8.226 963	9.584 865	4	6

[a] Relative intensities for peaks with interferences could not be determined. Relative intensities were measured on a multichannel spectrometer; thus, differing wavelength regions have differing efficiencies. Properties of the transitions (A, E, g) are reported from the NIST Atomic Spectra Database.[16]

912.80 nm were identified. In helium, these peaks had no interferences; however, in argon, the 911.89 and 912.80 nm emissions were lost within the argon 912.30 nm emission. The iodine 804.37 nm emission peak was identified in argon but had a slight interference with the argon 804.61 nm emission. The iodine 206.16 nm UV emission was resolved in both bulk gases; this peak theoretically should have a much stronger intensity than the other identified iodine peaks (*e.g.*, 2.8× the 905.83 nm intensity) based on its transition probability, degeneracy, and reduced upper energy level. However, due to the reduced sensitivity of the UV spectrometer channel *versus* the near-infrared channel, the measured intensity was reduced. This lower intensity indicates that UV-optimized spectrometers could enhance the detection of iodine in inert bulk gas streams, but the measurements performed with the multichannel spectrometer in this study represent the realistic detection capabilities with a low-cost, broadband system.

Although iodine emission peaks were detected in helium and argon, none were found in air at the trace concentrations evaluated (*i.e.*, ≤100 ppm). While further research dedicated to exploring this behavior is needed there are likely several variables involved. These may include reduced UV light transmission due to atmospheric absorbance, reduced excitation of iodine due to the rapid quenching in air plasmas, or it may be related to the excitation process itself in monoatomic inert gases *versus* the polyatomic molecules in air. Future studies examining the plasma properties of these different bulk gases containing iodine, as well as the spatiotemporal evolution of the plasma would provide better insight into the excitation mechanisms. Regardless of the cause, calibration in air was not performed due to a lack of iodine signal. An overlay of air, helium, and argon spectra containing nominally 70 ppm iodine at wavelength regions of interest is provided in Fig. S5. Fortunately, the detection of trace iodine in inert gases is still highly

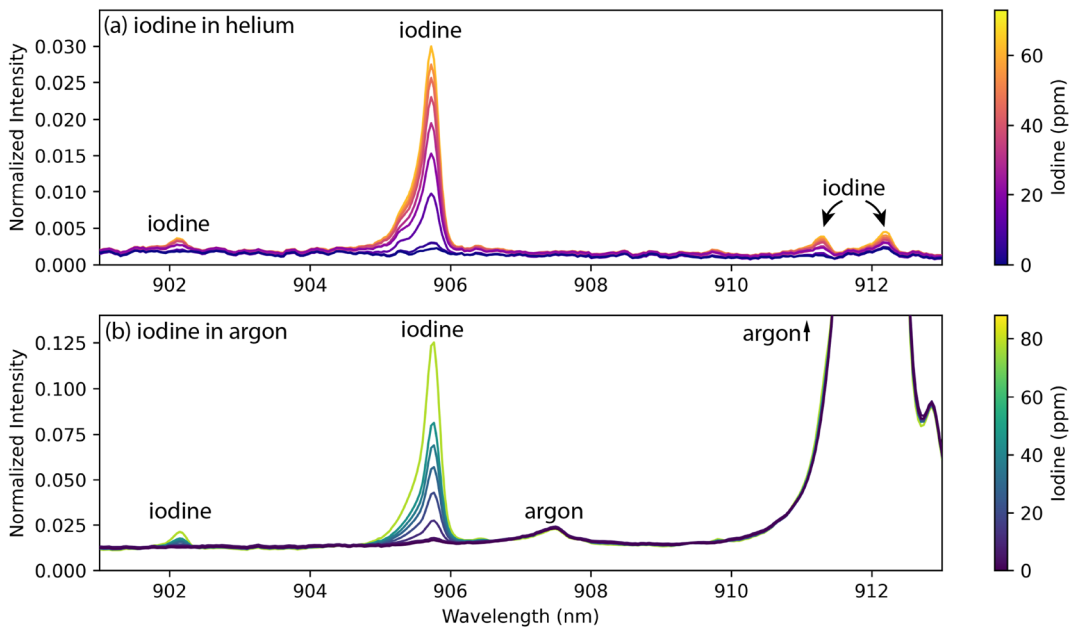

Fig. 2 Overlaid LIBS spectra of various concentrations of trace iodine in (a) helium and (b) argon, highlighting the strongest iodine emission peak window.

 This journal is © The Royal Society of Chemistry 2026

Open Access Article. Published on 13 January 2026. Downloaded on 2/25/2026 11:40:18 AM.
This article is licensed under a Creative Commons Attribution-NonCommercial 3.0 Unported Licence.

relevant to nuclear processes such as MSR off-gas systems and molten salt reprocessing of used nuclear fuel.

Optimization of LIBS collection settings

Due to the temporal behavior of laser-induced plasmas, the quality of LIBS measurements is subject to the time window in which they are measured relative to the lifetime of the plasma. Thus, before constructing calibration models, the LIBS collection settings were optimized for each bulk gas. LIBS measurements were repeated in helium and argon gas streams containing approximately 70 ppm iodine with delay times ranging from 1 to 50 μs. Because of the inability to gate the multichannel spectrometer at short exposure times, the exposure time was held constant at 1 ms (*i.e.*, infinity relative to the plasma lifetime). The SNR was calculated at each delay time, and the measurement window, which optimized the SNR of the 905.83 nm peak, was selected for further use. The LIBS spectra and calculated SNRs for the 905.83 nm iodine peak are shown in Fig. 3.

LIBS plasmas in helium and argon gas streams exhibit very different behavior because of their differences in ionization energies. Previous work explored the differences in laser-induced plasmas formed in the two bulk gases. These studies found that (1) the use of argon results in plasma temperatures nearly double those of helium, (2) electron densities in argon are typically an order of magnitude greater than those in He, and (3) argon plasma lifetimes are much greater than those of helium plasma.[21] These findings are reflected in the optimization of the iodine 905.83 nm signal shown in Fig. 3. The emission intensities of iodine peaks in argon were much greater than those measured in helium. This result is reflected in the maximum SNR in argon being nearly double what was measured in helium. Furthermore, the SNR fell much faster in helium compared to argon. These differences between the two bulk gases manifest in the optimal delay times being very different: 1 μs in helium and 10 μs in argon.

Calibration models, LODs, and real-time demonstration

After the optimal measurement conditions were determined, calibrations were performed to assess the LODs for iodine in the different bulk gases. These calibrations were performed by incrementally reducing the iodine concentration stepwise until no iodine signal was detected. Accumulated spectra (100 shots, 5 s) were collected at each concentration. Univariate models were built for the four iodine emission peaks detected in both bulk gases without major interferences (206.16, 804.37, 902.24, and 905.83 nm).

The helium dataset was processed as follows: (1) normalized to the 728.2 nm helium peak to account for variation in laser energy/plasma formation; (2) smoothed using a three-point window, first-order Savitzky–Golay filter to reduce noise; and (3) summed into 500-shot accumulations. Using 500-shot accumulations was selected to balance noise reduction and time resolution (25 s). The calibration models for iodine peaks in helium are shown in Fig. 4. For the weaker emission peaks (206.16 and 902.24 nm), the measurement precision decreases

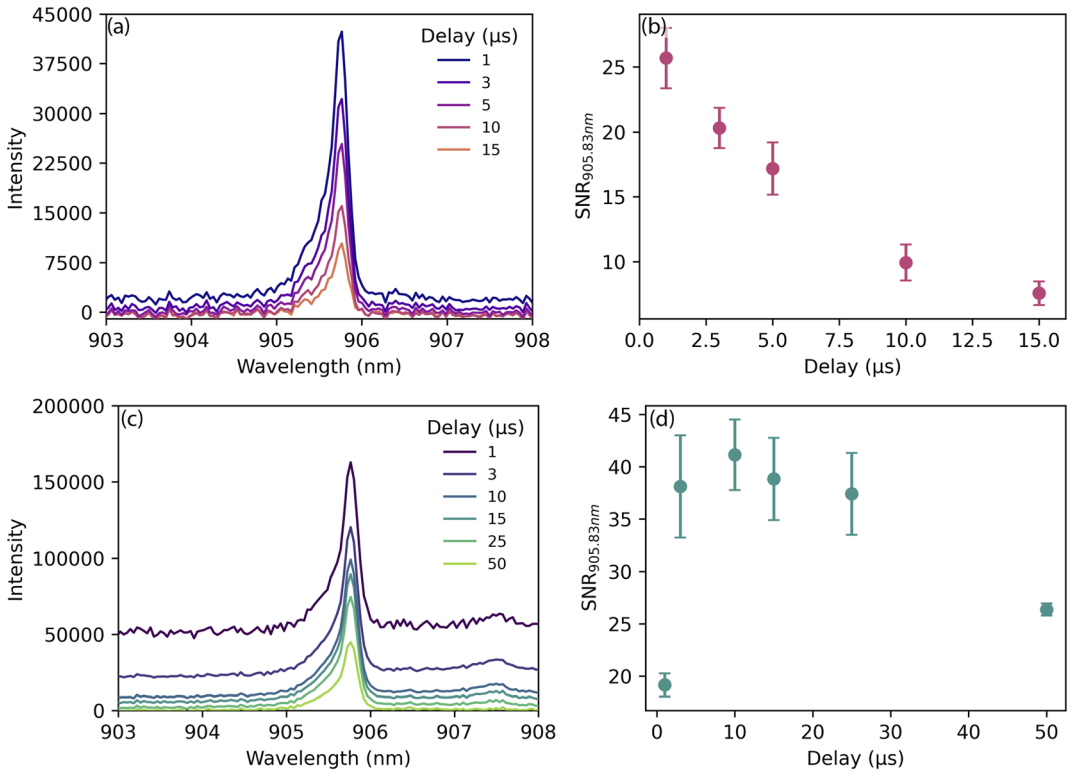

Fig. 3 Iodine 905.83 nm LIBS signal *versus* delay time in (a) helium and (c) argon. The calculated SNRs are shown in (b) helium and (d) argon.

Open Access Article. Published on 13 January 2026. Downloaded on 2/25/2026 11:40:18 AM.
This article is licensed under a Creative Commons Attribution-NonCommercial 3.0 Unported Licence.

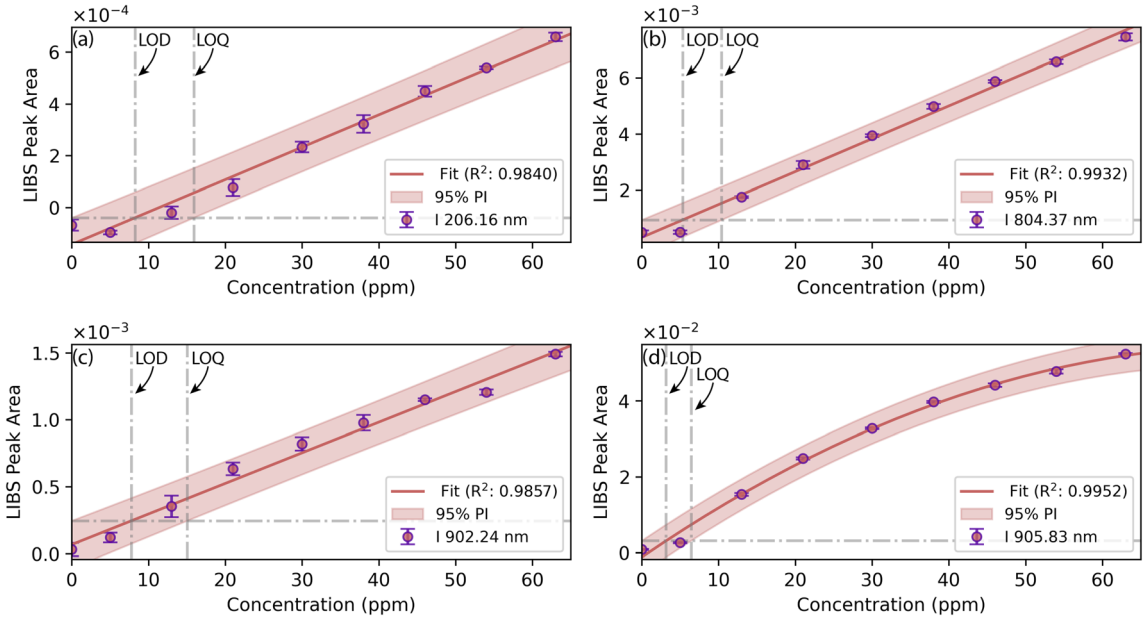

Fig. 4 Calibration models for trace iodine quantification in a helium bulk gas using the (a) 206.16, (b) 804.37, (c) 902.24, and (d) 905.83 nm iodine peaks. LIBS measurements were performed using a delay time of 1 μs and a gate width of 1 ms.

as the concentration falls. These peaks also have higher LODs compared to the stronger emissions (Table 2). The 804.37 nm peak shows excellent precision and linearity. Finally, the strongest emission peak, 905.83 nm, shows excellent precision; however, the calibration model shows nonlinear behavior, tilting around 80 ppm. Thus, this peak was fit with a second-order fit to properly consider its prediction band when assessing its associated LOD.

The argon dataset was processed in a similar fashion: (1) normalized to the 912.30 nm argon peak to account for variation in laser energy/plasma formation; (2) smoothed using a two-point window, first-order Savitzky–Golay filter to reduce noise; and (3) summed into 500-shot accumulations. The calibration models for iodine peaks in argon are shown in Fig. 5. Overall, the measurement precision in the argon bulk gas measurements was reduced compared to those in the helium bulk gas; however, the LODs for the helium calibrations were generally on par with their argon counterparts. The slight increase in the LOD for the 804.37 nm iodine peak can be attributed to the interference with the argon peak shoulder (Fig. S4). The other major difference between the two bulk gases is the behavior of the 905.83 nm iodine peak. In argon, the nonlinear behavior was not seen in the concentration regime that was studied. This different behavior is likely associated with the different plasma temperatures, electron density, and plasma self-absorption in the two gases.

The figures of merit for iodine calibrations in helium and argon are summarized in Table 2. All models resulted in strong linear fits with $R^2 > 0.95$. For all emission peaks in both bulk gases, the LODs, determined from their prediction bands, fall below 10 ppm. Beyond detection, the LOQs fall within 10–16 ppm; this range indicates the potential for LIBS to monitor trace gas-phase iodine without overly specialized spectrometers or low-pressure gas cells. The % RMSEC values were compared to determine which peak would best be used for prediction. For helium, the % RMSEC values of the 206.16, 804.37, and 902.24 nm peaks fall into the satisfactory category, indicating they would be useful for tracking changes but not optimal for accurate quantification. The 905.83 nm peak % RMSEC value falls below 5% in helium, signifying it would be the best emission for analytical measurements, although the second-order behavior of this peak would prevent the model from being extrapolated beyond the range of the calibration sample concentrations. In argon, the 206.16 and 902.24 nm models show slightly improved % RMSEC values due to their increased intensities (Table 1). Again, the 905.83 nm peak exhibits strong predictive capabilities with a % RMSEC below 5%; however, in

Table 2 Figures of merit for iodine LIBS calibration models in different bulk gases

	I 206.16 nm	I 804.37 nm	I 902.24 nm	I 905.83 nm
Helium				
R^2	0.9840	0.9932	0.9857	0.9952
LOD	8	5	8	3
LOQ	16	10	15	6
RMSEC	2.65	1.72	2.5	0.9
% RMSEC	8.4%	5.5%	7.9%	2.9%
Argon				
R^2	0.9893	0.9921	0.9938	0.9959
LOD	8	7	6	5
LOQ	16	13	12	10
RMSEC	2.48	2.13	1.89	1.53
% RMSEC	6.4%	5.5%	4.8%	3.9%

This journal is © The Royal Society of Chemistry 2026

Open Access Article. Published on 13 January 2026. Downloaded on 2/25/2026 11:40:18 AM.
This article is licensed under a Creative Commons Attribution-NonCommercial 3.0 Unported Licence.

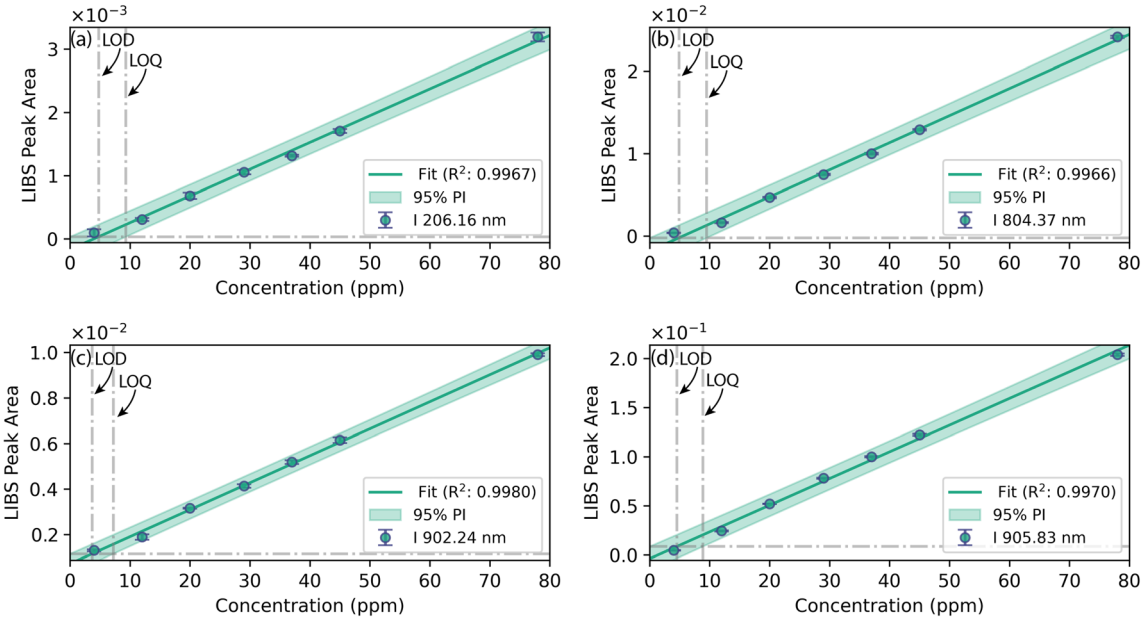

Fig. 5 Calibration models for trace iodine quantification in an argon bulk gas using the (a) 206.16, (b) 804.37, (c) 902.24, and (d) 905.83 nm iodine peaks. LIBS measurements were performed using a delay time of 10 μs and a gate width of 1 ms.

argon, this model is linear, which would allow for cautious extrapolation.

As further demonstration that LIBS can be used for real-time monitoring of iodine in gas streams, the iodine 905.83 nm model was applied to the entire data series collected during the argon calibration. The concentration predictions for this test are shown in Fig. 6. The highlighted green regions indicate where the spectral signals stabilized and were used for the calibration model. This data series encompasses >1 hour of nearly continuous monitoring and transient periods when the iodine concentration was varied.

In the absence of a secondary quantification technique, a gas mixture model was used to provide comparative concentration transient profiles. Using the concentration change between 25–35 min, the time constant for the gas system was estimated to be nominally 1 min. This time constant was then used to model the mixing gas concentration using the known concentration steps. As seen in Fig. 6, the LIBS calibration model clearly resolves the changes in flow rate ratios caused by concentration changes. The prediction precision also appears stable, corresponding to the strong predictive performance, as indicated by the % RMSEC value shown in Table 2. However, the LIBS model does begin to underpredict iodine concentrations at low

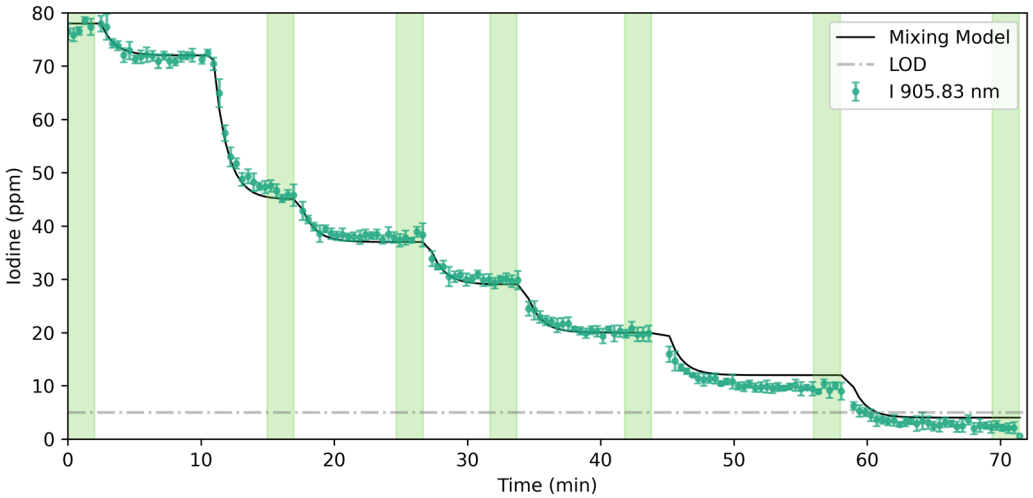

Fig. 6 Iodine concentrations predicted using the iodine 905.83 nm model over the duration of a calibration run. The green highlighted regions correspond to the spectra used for calibrating the iodine model. A gas mixture model (time constant = 1 min) was used to generate anticipated concentration transients for comparison. Error bars represent the standard deviation of the predictions (n = 5).

Open Access Article. Published on 13 January 2026. Downloaded on 2/25/2026 11:40:18 AM. This article is licensed under a Creative Commons Attribution-NonCommercial 3.0 Unported Licence.

concentrations (<20 ppm) as the LOD is approached. Finally, because this demonstration was performed only using the near-infrared channel in the multichannel spectrometer, which also covers the wavelengths needed for noble gas monitoring, the potential exists for a significantly reduced form factor for a LIBS monitoring system tailored for noble gases and iodine.[21]

Conclusion

Iodine is an element of high significance in nuclear applications due to its long half-life, volatile nature, and high biological activity. Thus, detecting iodine as a gas is essential for capture and abatement. For MSR and nuclear fuel recycling applications, iodine is anticipated to evolve into the off-gas system, where its capture is required by government regulations. Gas-phase iodine is a challenging analyte to monitor using most traditional analytical methods; thus, this study was performed to (1) assess the capability of LIBS to detect gas-phase iodine in flowing air, Ar, and He matrices; (2) optimize the LIBS measurement parameters for trace gas-phase iodine analysis using a multichannel spectrometer; and (3) use a single compact spectrometer to perform calibrations in the various bulk gases and quantify LODs relevant to online monitoring.

Gas-phase iodine was successfully measured in argon and helium matrices, although it was not detected at trace concentrations in air. This lack of detection in air requires further investigation as it likely relates to the excitation mechanisms of the iodine in air *versus* inert gases. Additionally, an emission line survey was reported to serve as a reference for future gas-phase iodine studies. LIBS plasmas vary greatly depending on the bulk gas used, requiring different collection settings in each gas. The optimal delay times were determined to be 1 and 10 μs in helium and argon, respectively. This result corresponds to the expected plasma lifetime of helium being short and argon being long. Following this optimization, calibration models were developed in each gas with calculated LODs as low as 3 ppm in helium and 5 ppm in argon. Finally, the strongest model (iodine 905.83 nm) was applied to a time series dataset collected in argon. The resulting prediction trace demonstrated the feasibility of real-time quantification of trace iodine in flowing inert gas systems, particularly relevant to molten salt applications.

Although this study successfully demonstrated the potential for real-time monitoring of trace iodine in inert flowing gases, several future improvements will need to be explored and further considered before field deployment. Specifically, the spectral behavior of iodine in sample streams containing a more complex composition (*e.g.*, noble gases, aerosols) should be explored to understand matrix effects and potential suppression of iodine emission peaks from other species. Additionally, alternate equipment may result in enhanced sensitivity. For example, inert gas-purged UV spectrometers may enhance the intensity of the 206.16 nm peak, which is theoretically the strongest iodine emission peak between 200 and 1000 nm. Furthermore, spectrometers with intensified charge-coupled device detectors have been demonstrated to enhance the sensitivity of LIBS measurements (particularly halides), although this benefit comes at the sacrifice of spectral coverage because these spectrometers can typically only monitor reduced wavelength ranges. For cases where very low iodine concentrations need be monitored, laser-induced fluorescence may be performed directly on the LIBS plasma to further pump transitions of interest.

Author contributions

Conceptualization (H. B. A., K. R. J.), data curation (H. B. A., Z. B. K., K. R. J., C. C. C.), formal analysis (H. B. A., Z. B. K.), funding acquisition (H. B. A., K. R. J., J. M.), investigation (H. B. A., Z. B. K.), methodology (H. B. A., Z. B. M.), visualization (H. B. A.), writing – original draft (H. B. A.), writing – review & editing (all authors).

Conflicts of interest

There are no conflicts to declare.

Data availability

All relevant data that support these experimental findings are available from the corresponding author upon reasonable request.

Supplementary information (SI) is available. See DOI: https://doi.org/10.1039/d5ja00481k.

Acknowledgements

The authors would like to acknowledge Jacquelyn Demink for assistance with graphics. This work was funded by the US Department of Energy's Office of Nuclear Energy, Advanced Reactor Development Program, Molten Salt Reactor Program and the Materials Recovery and Waste Form Development Program.

References

1 H. B. Andrews, J. McFarlane, A. S. Chapel, N. D. B. Ezell, D. E. Holcomb, D. de Wet, M. S. Greenwood, K. G. Myhre, S. A. Bryan and A. Lines, *Nucl. Eng. Des.*, 2021, **385**, 111529.
2 C. L. Beck, J. Cervantes, S. Chiswell, A. T. Greaney, K. R. Johnson, T. G. Levitskaia, L. R. Martin, G. McDaniel, S. Noble and J. M. Rakos, *RSC Adv.*, 2024, **14**, 35255–35274.
3 R. Ngelale, J. McFarlane, D. Orea and K. R. Johnson, *React. Chem. Eng.*, 2025, **10**, 2225–2237.
4 K. R. Johnson, C. Cobble, J. Mcfarlane, K. M. Peruski, D. Glasgow, B. K. Vestal, H. Meyer III, E. MacLaughlin and S. Thomas, *Iodine Capture Studies of Silver Mordenite and Novel Alternative Metal Sorbents, ORNL/TM-2024/3588*, Oak Ridge National Laboratory (ORNL), Oak Ridge, TN (United States), 2024.
5 K. Eisawi, E. Loni, S. Chong, M. Liezers, M. Tang, K. S. Brinkman, B. J. Riley and M. Naguib, *Adv. Mater. Interfaces*, 2025, 2500011.

 This journal is © The Royal Society of Chemistry 2026

Open Access Article. Published on 13 January 2026. Downloaded on 2/25/2026 11:40:18 AM.
This article is licensed under a Creative Commons Attribution-NonCommercial 3.0 Unported Licence.

6 S. Chong, B. J. Riley, K. Baskaran, S. Sullivan, L. El Khoury, K. Carlson, R. M. Asmussen and M. S. Fountain, *New J. Chem.*, 2024, **48**, 9880–9884.
7 B. J. Riley, C. L. Beck, J. S. Evarts, S. Chong, A. M. Lines, H. M. Felmy, J. McFarlane, H. B. Andrews, S. A. Bryan and K. C. McHugh, *AIP Adv.*, 2024, **14**, 080701.
8 H. Andrews, J. Mcfarlane, D. Holcomb, N. D. Ezell, K. Myhre, A. Lines, S. Bryan and H. M. Felmy, *Sensor Technology for Molten Salt Reactor Off-Gas Systems, Oak Ridge National Laboratory (ORNL)*, Oak Ridge, TN (United States), 2021, DOI: 10.13182/T124-34454.
9 S. Kireev, S. Shnyrev, I. Sobolevsky and A. Kondrashov, *Laser Phys. Lett.*, 2014, **12**, 015701.
10 S. Kireev, S. Shnyrev and I. Sobolevsky, *Laser Phys. Lett.*, 2016, **13**, 065701.
11 S. Kireev, S. Shnyrev and S. Suganeev, *Laser Phys.*, 2016, **26**, 095604.
12 H. M. Felmy, A. J. Clifford, A. S. Medina, R. M. Cox, J. M. Wilson, A. M. Lines and S. A. Bryan, *Environ. Sci. Technol.*, 2021, **55**, 3898–3908.
13 E. H. Kwapis, J. Borrero, K. S. Latty, H. B. Andrews, S. S. Phongikaroon and K. C. Hartig, *Appl. Spectrosc.*, 2024, **78**, 9–55.
14 D. A. Cremers and L. J. Radziemski, *Anal. Chem.*, 1983, **55**, 1252–1256.
15 Y. Ralchenko, *Memor. Soc. Astronom. Ital. Suppl.*, 2005, **8**, 96.
16 A. Kramida, K. Olsen and Y. Ralchenko, *National Institute of Standards and Technology*, US Department of Commerce, 2019.
17 X. Zhang, Y. Deguchi, Z. Wang, J. Yan and J. Liu, *J. Anal. At. Spectrom.*, 2014, **29**, 1082–1089.
18 Q. Zhang, Y. Liu, Y. Chen, Y. Zhangcheng, Z. Zhuo and L. Li, *Opt. Express*, 2020, **28**, 22844–22855.
19 N. A. H. Poole and A. I. Hawari, *ANS Trans.*, 2025, **133**(1), 402–405.
20 M. Gaft, L. Nagli, Y. Raichlin, F. Pelascini, G. Panzer and V. M. Ros, *Spectrochim. Acta, Part B*, 2019, **157**, 47–52.
21 H. B. Andrews, Z. B. Kitzhaber and J. McFarlane, *Spectrochim. Acta, Part B*, 2025, 107237.
22 H. B. Andrews, Z. B. Kitzhaber, D. Orea and J. McFarlane, *J. Am. Chem. Soc.*, 2024, **147**, 910–917.
23 Z. B. Kitzhaber, D. Orea, J. McFarlane, B. T. Manard and H. B. Andrews, *ACS Omega*, 2025, **10**, 37889–37897.
24 D. W. Hahn and N. Omenetto, *Appl. Spectrosc.*, 2012, **66**, 347–419.
25 H. B. Andrews and L. R. Sadergaski, *Talanta*, 2023, **259**, 124554.
26 J.-M. Mermet, *Spectrochim. Acta, Part B*, 2008, **63**, 166–182.
27 M. McCusker, in *Excimer Lasers*, Springer, 2005, pp. 47–86.